

This item is the archived peer-reviewed author-version of:

An additional Lrp4 high bone mass mutation mitigates the sost-knockout phenotype in mice by increasing bone remodeling

Reference:

Hendrickx Gretl, Boudin Eveline, Mateiu Ligia, Yorgan Timur A., Steenackers Ellen, Kneissel Michaela, Kramer Ina, Mortier Geert, Schinke Thorsten, Van Hul Wim.- An additional Lrp4 high bone mass mutation mitigates the sost-knockout phenotype in mice by increasing bone remodeling
Calcified tissue international - ISSN 1432-0827 - New york, Springer, 114:2(2024), p. 171-181
Full text (Publisher's DOI): <https://doi.org/10.1007/S00223-023-01158-0>
To cite this reference: <https://hdl.handle.net/10067/2021360151162165141>

1 **An additional *Lrp4* high bone mass mutation mitigates**
2 **the *Sost*-knockout phenotype in mice by increasing bone remodeling**

3 *Gretl Hendrickx^{1,2}, Eveline Boudin¹, Ligia Mateiu¹, Timur A. Yorgan³, Ellen Steenackers¹, Michaela*
4 *Kneissel⁴, Ina Kramer⁴, Geert Mortier^{1,2}, Thorsten Schinke³, Wim Van Hul¹*

5 ¹ *Centre for Medical Genetics, University and University Hospital of Antwerp, Antwerp, Belgium*

6 ² *Department of Human Genetics, KU Leuven, Leuven, Belgium*

7 ³ *Department of Osteology and Biomechanics, University Medical Center Hamburg-Eppendorf,*
8 *Hamburg, Germany*

9 ⁴ *Diseases of Aging and Regenerative Medicine, Novartis Institutes for BioMedical Research, Basel,*
10 *Switzerland.*

11
12 **Correspondence to:**

13 Wim Van Hul; wim.vanhul@uantwerpen.be

14
15 **Gretl Hendrickx:** 0000-0001-6715-9241

16 **Eveline Boudin:** 0000-0003-4818-6804

17 **Ligia Mateiu:** 0000-0002-2655-3581

18 **Timur A. Yorgan:** 0000-0002-0712-0983

19 **Geert Mortier:** 0000-0001-9871-4578

20 **Thorsten Schinke:** 0000-0002-8576-0177

21 **Wim Van Hul:** 0000-0002-5065-7858

22
23 **Key words:** *Lrp4; Sost; sclerostin; sclerosteosis; high bone mass; RNA sequencing*

24
25 **Statements and Declarations**

26 **Conflict of interest**

27 GH, EB, LM, TAY, ES, GM, TS and WVH declare that they have no conflict of interest. MK
28 and IK are employees of Novartis Institutes for BioMedical Research.

29
30 **Ethical approval**

31 All animal experimental procedures were carried out in compliance with the ARRIVE
32 guidelines and were approved by the University of Antwerp Ethics Committee (reference
33 number 2017-60).

34

35

1 **Funding**

2 This research was funded by grants of the Fund for Scientific Research Flanders (FWO grant
3 G031915N), a personal grant to EB (FWO personal grant 12A3814N), a research grant of the University
4 of Antwerp (Methusalem—OEC grant—“GENOMED”; FFB190208) and the European Community’s
5 Seventh Framework Programme (FP7/2007-2013) under grant agreement no. 602300 (SYBIL).

6 **Contributions**

7 Conceptualization, GH, EB and WVH; Data curation, GH and EB; Formal analysis, GH, EB, LM and
8 TAY ; and Methodology, GH, EB, LM, TAY and ES; Supervision, WVH; Validation, GH, EB and LM;
9 Writing—original draft, GH and WVH; Writing—review & editing, GH, EB, LM, TAY, ES, MK, IK,
10 GM, TS and WVH. All authors listed have made a substantial, direct, and intellectual contribution to
11 the work and have approved it for publication. All authors have read and agreed to the published version
12 of the manuscript.

1 **Abstract**

2 Pathogenic variants disrupting the binding between sclerostin (encoded by *SOST*) and its receptor LRP4
3 have previously been described to cause sclerosteosis, a rare high bone mass disorder. The sclerostin-
4 LRP4 complex inhibits canonical WNT signaling, a key pathway regulating osteoblastic bone formation
5 and a promising therapeutic target for common bone disorders, such as osteoporosis. In the current study,
6 we crossed mice deficient for *Sost* (*Sost*^{-/-}) with our p.Arg1170Gln *Lrp4* knock-in (*Lrp4*^{KI/KI}) mouse
7 model to create double mutant *Sost*^{-/-};*Lrp4*^{KI/KI} mice. We compared the phenotype of *Sost*^{-/-} mice with
8 that of *Sost*^{-/-};*Lrp4*^{KI/KI} mice, to investigate a possible synergistic effect of the disease-causing
9 p.Arg1170Trp variant in *Lrp4* on *Sost* deficiency. Interestingly, presence of *Lrp4*^{KI} alleles partially
10 mitigated the *Sost*^{-/-} phenotype. Cellular and dynamic histomorphometry did not reveal mechanistic
11 insights into the observed phenotypic differences. We therefore determined the molecular effect of the
12 *Lrp4*^{KI} allele by performing bulk RNA sequencing on *Lrp4*^{KI/KI} primary osteoblasts. Unexpectedly,
13 mostly genes related to bone resorption or remodeling (*Acp5*, *Rankl*, *Mmp9*) were upregulated in
14 *Lrp4*^{KI/KI} primary osteoblasts. Verification of these markers in *Lrp4*^{KI/KI}, *Sost*^{-/-} and *Sost*^{-/-};*Lrp4*^{KI/KI} mice
15 revealed that sclerostin deficiency counteracts this *Lrp4*^{KI/KI} effect in *Sost*^{-/-};*Lrp4*^{KI/KI} mice. We therefore
16 hypothesize that models with two inactivating *Lrp4*^{KI} alleles rather activate bone remodeling, with a net
17 gain in bone mass, whereas sclerostin deficiency has more robust anabolic effects on bone formation.
18 Moreover, these effects of sclerostin and *Lrp4* are stronger in female mice, contributing to a more severe
19 phenotype than in males and more detectable phenotypic differences among different genotypes.

1 Introduction

2 After decades of research, WNT signalling is considered a master regulator of skeletal homeostasis, and
3 canonical or WNT/ β -catenin signalling in particular an essential regulator of osteoblastic bone formation
4 [1]. The latter has been supported by the identification of disease-causing variants in several components
5 of the canonical WNT pathway in patients with high bone mass (HBM) disorders, also known as
6 sclerosing bone dysplasias [2]. Causal variants have been identified in genes encoding extracellular
7 regulators (*SOST*), co-receptors (*LRP4*, *LRP5*, *LRP6*) or intracellular regulators (*AMER1*, *CTNNB1*),
8 contributing to unique HBM phenotypes, but generally sharing an increased activation of the canonical
9 WNT pathway and induced osteoblastic bone formation [2].

10 Sclerosteosis is such a monogenic HBM disorder with an autosomal recessive inheritance pattern and
11 marked by a generalized and progressive HBM, especially at the skull and tubular bones, macrocephaly
12 and syndactyly [3]. Disease-causing variants have so far been identified in both *SOST* (MIM 269500)
13 or *LRP4* (MIM 614305) [4-6]. These genes also reveal the affected underlying molecular mechanism,
14 i.e. the interaction of the WNT antagonist sclerostin (encoded by *SOST*) with its receptor LRP4 (encoded
15 by *LRP4*). Loss-of-function (LoF) variants in *SOST* that have been identified in sclerosteosis patients
16 were reported to result in lower or even absent levels of sclerostin [7]. As an inhibitor of canonical WNT
17 signaling, *SOST* LoF variants will therefore reduce the inhibition of the pathway, resulting in an
18 increased osteoblastic bone formation, and a progressively dense skeleton. For *LRP4*, hypomorphic
19 missense variants were initially only localised in the third β -propeller domain of the receptor [6, 8].
20 Deeper investigations revealed a sclerostin-interacting pocket in this region, and the mutations found by
21 us and others (p.Arg1170Gln, p.Arg1170Trp and p.Trp1186Ser) were therefore proposed to specifically
22 impair interaction with sclerostin and hence its inhibitory function on canonical WNT signaling [6, 8,
23 9]. Recently however, we reported that compound heterozygous variants in the 1st and 3rd β -propeller
24 domain of LRP4 can also result in a sclerosteosis phenotype, broadening this receptor's mutational and
25 mechanistic spectrum [10]. In addition, not only sclerostin but also other known modulators of canonical
26 WNT signaling and bone metabolism e.g. Wise and Dickkopf1 (*DKK1*) are reported to interact with
27 LRP4 [11, 12].

28 Both *SOST* and *LRP4* have been extensively studied in animal models to explore the underlying
29 molecular and cellular mechanisms contributing to the related sclerosteosis phenotypes. *Sost* knockout
30 (*Sost*^{-/-}) mice, for example, model the sclerosteosis-like HBM phenotype very well [13, 14]. On a cellular
31 level, these mice have numerous enlarged osteoblasts, producing larger amounts of bone matrix, which
32 led to the understanding that *Sost* deficiency has strong osteoanabolic effects. As for *Lrp4*, two specific
33 knock-in models have been generated and studied by us (*Lrp4*^{Arg1170Gln}) [15] and others (*Lrp4*^{Arg1170Trp})
34 [16]. Also here, cellular studies have identified the osteoblast as the leading cell type during disease
35 pathogenesis.

1 So far, findings in patients and animal models with *SOST*-related HBM phenotypes have inspired and
2 motivated the pharmaceutical industry towards the development of monoclonal antibodies against
3 sclerostin. Evidently, as reduced sclerostin levels have robust anabolic effects on osteoblastic bone
4 formation, sclerostin has been an attractive therapeutic target for patients suffering from low bone mass
5 and/or fragility fractures, such as osteoporosis. Currently, sclerostin neutralizing antibodies are
6 perceived as one the most potent osteoporosis drugs [17]. As osteoporosis is a very common disorder
7 affecting one in three women and one in five men above 55, this development has and will still have a
8 large impact on our ageing society [18]. Accordingly, the 3rd β -propeller domain of *Lrp4* has been
9 suspected to provide an additional opportunity to augment osteoblastic canonical WNT signaling for
10 therapeutic applications [19].

11 The primary goal of this study was to investigate a possible additive effect of the disease-causing
12 p.Arg1170Trp variant in *LRP4* on *SOST* deficiency. For this purpose, we crossed *Sost* knockout (*Sost*^{-/-}
13) with *Lrp4* knock-in (*Lrp4*^{KI/KI}) mice carrying the inactivating p.Arg1170Trp variant, to generate *Sost*^{-/-}
14 ;*Lrp4*^{KI/KI} mice for extensive phenotyping. Interestingly, we detected a milder HBM phenotype in
15 female, not male, *Sost*^{-/-};*Lrp4*^{KI/KI} mice than in *Sost*^{-/-} mice. Finally, RNA sequencing of *Lrp4*^{KI/KI}
16 primary osteoblasts was performed to provide us with unbiased molecular insights into the phenotypic
17 features and differences we detected. By using this approach, we detected an unexpected upregulation
18 of genes related to bone resorption and bone remodelling in *Lrp4*^{KI/KI} primary osteoblasts.

1 **Material and Methods**

2 **Animal models**

3 Two existing mutant (*Lrp4*^{Arg1170Gln} and *Sost*^{KO}) mouse lines were used to create a novel compound
4 mutant mouse line (*Sost*^{KO};*Lrp4*^{Arg1170Gln}) for this study. Generation and genotyping of the *Sost* knockout
5 (*Sost*^{-/-}) mouse model with a targeted disruption of the *Sost* coding region on a C57BL/6J background
6 was performed at Novartis and described elsewhere [13]. Standard PCR-based genotyping of *Sost*^{KO}
7 mice was done by using a mix of three primers; 5'-ACT CCA CAC GGT CTG GAA AGT GTT G-3';
8 5'-TCC ACA ACC AGT CGG AGC TCA AGG-3' and 5'-GGG TGG GAT TAG ATA AAT GCC TGC
9 TCT -3'. The *Lrp4*^{Arg1170Gln} knock-in mouse model, hereafter referred to as *Lrp4*^{KI} mice, on a C57BL/6N
10 background was previously generated for us at Polygene AG (Rümlang Switzerland) [15]. Briefly, the
11 LRP4 p.Arg1170 residue in humans corresponds to the *Lrp4* p.Arg1170 in mice and the same G to A
12 inactivating base pair change as found in sclerosteosis patients [9] was introduced in the mouse model,
13 resulting in the loss of a *SmaI* restriction site that can be used for genotyping. Initially, heterozygous
14 *Lrp4*^{+/Arg1170Gln} were crossed with heterozygous *Sost*^{+/-} mice to generate a novel compound mutant mouse
15 line. These double mutant mice were then used for further breeding to generate mice with two mutant
16 alleles of *Lrp4* and/or *Sost*.

17 **Animal husbandry and experiments**

18 All mice were held at the animal facility of the University of Antwerp and maintained on a 12h light-
19 dark cycle, with free access to regular chow and tap water. All animal experimental procedures were
20 carried out in compliance with the ARRIVE guidelines [20] and were approved by the University of
21 Antwerp Ethics Committee (reference number 2017-60). All following phenotypical analyses are
22 performed on 5-month-old male (n=6 per genotype) and female mice (n=3 per genotype). The genotypes
23 investigated in this study are *Sost*^{+/+};*Lrp4*^{+/+} (littermate controls), *Sost*^{+/-};*Lrp4*^{+KI}, *Sost*^{-/-};*Lrp4*^{+/+} (*Sost*
24 ^{-/-}) and *Sost*^{-/-};*Lrp4*^{KI/KI}.

25 **Radiological assessment**

26 The skeletons were dissected and fixed in 3.7% PBS-buffered formaldehyde for 24 hours after which
27 they were transferred into 80% ethanol for an initial analysis by contact X-ray (35 kV, 2 s; Faxitron
28 XRay Corp., USA). For μ CT analysis the right femur of each mouse was dissected from the fixed mouse,
29 before being placed into a radiotranslucent sample holder. Dehydration was prevented by filling the
30 holder with PBS. μ CT scanning and analysis was performed as previously described using a μ CT 40
31 desktop cone-beam microCT (Scanco Medical, CHE) [21] according to standard guidelines [22].

32 **Bone histology**

33 Vertebral bodies L1 to L4 and tibiae were dehydrated in ascending ethanol concentrations, before being
34 embedded into methylmethacrylate. Sections of 4 μ m thickness were cut in the sagittal plane (Microtec
35 rotation microtome) and stained by von Kossa/van Gieson (for static histomorphometry) or toluidine

1 blue (for cellular histomorphometry) as previously described [23]. To determine the bone formation
2 rate, all mice were injected with calcein (30mg/kg, i.p.) at 9 days and 2 days before euthanasia. Dynamic
3 histomorphometry was performed on unstained 12 μ m sections of the vertebral bodies. Static, cellular,
4 and dynamic histomorphometry at trabecular bone surfaces was carried out according to the guidelines
5 of the American Society for Bone and Mineral Research [24] using an OsteoMeasure system
6 (Osteometrics Inc., Decatur, GA, USA) and Bioquant Osteo software (BIOQUANT Image Analysis
7 Corp., Nashville, TN, USA) [21].

8 **Cell culture**

9 Primary osteoblasts were isolated from the long bones of *Sost*^{+/+};*Lrp4*^{+/+}, *Sost*^{+/+};*Lrp4*^{KI/KI} and *Sost*^{-/-}
10 ;*Lrp4*^{KI/KI} mice as described previously [25]. In brief, cleaned long bones were cut into small pieces and
11 incubated with 2 mg/ml collagenase II (Sigma) solution for 2 h at 37°C in a shaking water bath. Then,
12 the bone fragments were washed and cultured in α -MEM containing 10% FCS, 100 U/ml penicillin, 100
13 μ g/ml streptomycin, and 250 ng/ml amphotericin B in 25 cm² culture flasks. After confluence, bone
14 fragments were removed, the confluent layers were trypsinized and the cells were replated in 25 cm²
15 culture flasks until confluent.

16 **Expression analysis**

17 RNA from primary osteoblasts was isolated using the ReliaPrep RNA Cell Miniprep System (Promega
18 Corporation), and concentration and quality of total RNA were investigated using the Fragment
19 Analyzer System (Agilent Technologies). For expression analysis, 1 μ g of total RNA of high quality
20 (RNA Quality Number (RQN) \geq 7) from *Sost*^{+/+};*Lrp4*^{+/+} (n=3) and *Sost*^{+/+};*Lrp4*^{KI/KI} mice (n=3) was used
21 for RNA sequencing (Eurofins Genomics). Here, the RNA Seq library was prepared using the TruSeq
22 Stranded Total RNA Library Prep Kit (Illumina) and library validation was carried out using the Agilent
23 4200 TapeStation system (Agilent). RNA sequencing was carried out on an Illumina HiSeq platform
24 and data analysis was performed using the mm10, v102 release ENSEMBL genome annotation.
25 Differential gene expression was analyzed using DESeq2 [26]. The protein coding genes with an FDR-
26 corrected *P*-values $<$ 0.1 were considered significant. Gene set enrichment analysis was done with the
27 package fgSEA in R using the Molecular Signatures Database (MSigDB) C5 biological processes and
28 the C2 canonical pathways collection. For confirmation of differentially expressed genes with qRT-
29 PCR, total RNA was reverse transcribed to cDNA using the Superscript III First Strand Synthesis
30 System (Thermo Fisher Scientific) according to manufacturer's instructions. qPCR was performed using
31 the qPCR Core kits for SYBR Green I, No ROX (Eurogentec). Each sample was analyzed in triplicate
32 and *Gapdh* was included as reference gene (primer sequences available upon request). Relative
33 quantification was performed according to the Livak method, where results are expressed in the linear
34 form using the delta-delta comparative threshold cycle formula ($2^{-\Delta\Delta CT}$).

1 **Biochemical analysis**

2 After sacrifice at 5 months of age, blood was drawn with cardiac puncture and serum was isolated and
3 stored at -80°C. Serum levels of the same mice were determined using ELISA of procollagen type-I C-
4 terminal peptide (#SEA570Mu, PICP, Cloud-Clone Corp), collagen type 1 cross-linked C-telopeptide
5 (CTX-1, #AC-06F1, Ratlaps EIA detecting CTX from ImmunoDiagnostic Systems), sclerostin
6 (ab213889, Abcam), tartrate-resistant acid phosphatase (TRAP, LS-F54861, LifeSpanBiosciences Inc),
7 receptor activator of nuclear factor kappa-B ligand (RANKL, MTR00, R&D Systems) and
8 osteoprotegerin (OPG, M0P00, R&D Systems) according to the manufacturers' protocols.

9 **Statistical analysis**

10 Statistical analysis was performed by comparing multiple groups with different alleles of two
11 independent genetic loci, with a one-way ANOVA with Šidák's multiple comparison test (GraphPad
12 Software Inc., USA). All data are reported as the mean \pm SD with additional points representing
13 individual animals. A value of $P \leq 0.05$ was considered statistically significant.

1 **Results**

2 **Additional presence of *Lrp4^{KI}* alleles mitigate the *Sost^{KO}* high bone mass phenotype**

3 Five-month-old male and female *Sost^{+/+};Lrp4^{+/+}* (WT), *Sost^{+/-};Lrp4^{+KI}*, *Sost^{-/-};Lrp4^{+/+}* (*Sost^{-/-}*) and *Sost^{-/-};Lrp4^{KI/KI}* mice were collected for skeletal phenotyping. As a novel compound mutant mouse line, *Sost^{-/-};Lrp4^{KI/KI}* mice were viable and fertile.

6 We first performed μ CT analysis of the femoral bones from male (n=6) and female mice (n=3) to analyse
7 the structural properties of the cortical and trabecular bone compartments (Fig. 1). As for the cortical
8 bone, we detected a larger midshaft diameter (Ms.D) in male and female *Sost^{-/-}* femora and female *Sost^{-/-}*
9 *;Lrp4^{KI/KI}* mice, in comparison to controls (Fig. 1A-B). Cortical thickness (Ct.Th) was significantly
10 higher in male and female *Sost^{-/-}* and *Sost^{-/-};Lrp4^{KI/KI}* mice, compared to control mice. Interestingly, we
11 detected a lower Ct.Th in female *Sost^{-/-};Lrp4^{KI/KI}* mice than in *Sost^{-/-}* mice (Fig. 1C). Similarly, in the
12 trabecular bone compartment, we observed a significant larger trabecular bone volume (BV/TV) in male
13 and female *Sost^{-/-}* and *Sost^{-/-};Lrp4^{KI/KI}* mice compared to wildtype controls, whereas BV/TV was
14 significantly lower in female *Sost^{-/-};Lrp4^{KI/KI}* mice than in *Sost^{-/-}* mice (Fig. 1D-E). Generally, we did not
15 observe significant differences in the measured cortical or trabecular parameters in compound
16 heterozygous mutant lines, i.e. male or female *Sost^{+/-};Lrp4^{+KI}* mice, when compared to control mice
17 (Fig. 1).

18 In parallel, structural properties of the trabecular bone were verified using Von Kossa/van Gieson
19 histomorphometry on sections of the lumbar vertebral bodies (L1 to L4) and tibiae of all mutant mice
20 (Fig. 2). Both in the lumbar spine and tibiae, we detected a significant higher trabecular BV/TV in male
21 and female *Sost^{-/-}* and *Sost^{-/-};Lrp4^{KI/KI}* mice compared to controls, whereas an increase in the trabecular
22 thickness (Tb.Th) was only present in females (Fig. 2). Interestingly, only in the tibiae but not in the
23 vertebral bodies, BV/TV and Tb.Th values were significantly lower in female *Sost^{-/-};Lrp4^{KI/KI}* mice, in
24 comparison to female *Sost^{-/-}* mice (Fig. 2D). We again did not observe significant differences in any of
25 the investigated trabecular parameters in double heterozygous mutant lines, compared to controls (Fig.
26 2).

27 Altogether, structural analysis of the long bones (femur, tibia) and lumbar spine, using μ CT and
28 histology, shows that *Sost^{-/-}* and *Sost^{-/-};Lrp4^{KI/KI}* both present with a HBM phenotype in the cortical and
29 trabecular compartments. This osteosclerotic phenotype was overall similar for male mice of both
30 genotypes, but less severe in the long bones of female *Sost^{-/-};Lrp4^{KI/KI}* mice, than in *Sost^{-/-}* mice.

31

32

33

34 **Cellular histomorphometry and serum biomarker analysis of *Sost^{-/-}* and *Sost^{-/-};Lrp4^{KI/KI}* mice**

1 Based on the structural differences that we observed between *Sost*^{-/-} and *Sost*^{-/-};*Lrp4*^{KI/KI} mice, and lack
2 of differences in the heterozygous mutant mouse lines, we focused on homozygous *Sost*^{-/-} and *Sost*^{-/-}
3 ;*Lrp4*^{KI/KI} mice for the remainder of our study.

4 Cellular histomorphometry was performed to detect potential cellular defects underlying the phenotypic
5 differences that we described with μ CT and histology. Quantification of the osteoblast number
6 (N.Ob/B.Pm) and osteoblast-covered surface (Ob.S/BS) demonstrated no significant differences for *Sost*^{-/-}
7 and *Sost*^{-/-};*Lrp4*^{KI/KI} mice, compared to WT controls and between both mutant models (Fig. 3A). There
8 was however a trend towards a higher Ob.S/BS ($P=0.06$) in male *Sost*^{-/-};*Lrp4*^{KI/KI} mice, compared to WT
9 mice (Fig. 3A). Osteoblast activity, which we quantified by using dynamic histomorphometry of the
10 bone formation rate per bone surface area (BFR/BS), was significantly higher in male *Sost*^{-/-} and *Sost*^{-/-}
11 ;*Lrp4*^{KI/KI} mice, compared to controls (Fig. 3B). Similar tendencies were observed in female mice,
12 however since non-evaluable samples reduced the group sizes, reliable statistical testing could not be
13 performed. Histomorphometry of the osteoclasts indicated a lower osteoclast number (N.Oc/B.Pm) and
14 osteoclast-covered surface (Oc.S/BS) in *Sost*^{-/-} and *Sost*^{-/-};*Lrp4*^{KI/KI} mice, compared to WT mice (Fig.
15 3C). We did not observe significant differences between *Sost*^{-/-} and *Sost*^{-/-};*Lrp4*^{KI/KI} mice. In parallel, we
16 quantified bone formation (PICP) and resorption (CTX-1) markers in the serum of five-month-old
17 controls, *Sost*^{-/-} and *Sost*^{-/-};*Lrp4*^{KI/KI} mice by using ELISA. These biochemical analyses revealed a
18 significant higher level of PICP in female *Sost*^{-/-};*Lrp4*^{KI/KI} mice, in comparison to controls (Fig. 3D).
19 Again, no differences between serum markers of *Sost*^{-/-} and *Sost*^{-/-};*Lrp4*^{KI/KI} mice of both genders were
20 detected.

21 Our cellular and dynamic analyses shows an induction of osteoblast activity and a reduction in
22 osteoclast-related parameters in *Sost*^{-/-} and *Sost*^{-/-};*Lrp4*^{KI/KI} mice, whereas either mild or no differences
23 were found in bone formation or resorption serum markers in these mice.

24 **Transcriptome-wide expression analysis of *Lrp4*^{KI/KI} osteoblasts reveals upregulation of genes** 25 **related to bone resorption and remodeling**

26 Skeletal phenotyping of *Sost*^{-/-} and *Sost*^{-/-};*Lrp4*^{KI/KI} demonstrated that the additional presence of two
27 *Lrp4*^{KI} alleles affects the integrity of the *Sost*^{-/-} HBM phenotype, especially in female mice. We could
28 however not explain these phenotypic differences by standard cellular and biochemical analyses (Fig.
29 3).

30 To improve our understanding of the effect of *Lrp4*^{KI} alleles on a molecular level, we next performed
31 bulk RNA sequencing on three independent sets of primary long bone osteoblasts of *Lrp4*^{+/+} and
32 *Lrp4*^{KI/KI} mice. Here, looking at the adjusted P-values, only 14 genes showed a significant differential
33 expression in *Lrp4*^{KI/KI} primary osteoblasts, in comparison to *Lrp4*^{+/+} osteoblasts (Fig. 4A-B). Most of
34 these genes, unexpectedly, seemed to be related to osteoclast biology at first sight, e.g. *Mmp9*, *Acp5*
35 (also known as *Trap*), *Dcstamp*, *Oscar* and *Tnfsf11* (also known as *Rankl*) (Fig. 4B). In line with this,

1 gene ontology (GO) pathway analysis demonstrated a significant enrichment of genes related to
2 osteoclast differentiation or activity (Fig. 4C). ‘Positive regulation of osteoclast differentiation’
3 (GO:0045672) was the most enriched biological process in *Lrp4^{KI/KI}* osteoblasts, with a normalized
4 enrichment score (NES) of 2.22. Other significantly enriched biological processes related to bone
5 resorption were ‘osteoclast development’ (GO:0036035; NES 2.12), ‘bone resorption’ (GO:0045453;
6 NES 2.07), ‘regulation of osteoclast development’ (GO:2001204; NES 2.04), ‘keratan sulfate catabolic
7 process’ (GO:0042340; NES 1.94), ‘multinuclear osteoclast differentiation’ (GO:0072674; NES 1.89)
8 and ‘positive regulation of osteoclast development’ (GO:2001206; NES 1.85). On the other hand,
9 biological processes related to bone modelling (‘skeletal system development’; GO:0001501; NES 1.85)
10 or bone remodeling (‘positive regulation of tissue remodeling’; GO:0034105; NES 2.19 and ‘tissue
11 remodeling’; GO:0048771; NES 1.98) were significantly enriched in *Lrp4^{KI/KI}* osteoblasts (Fig. 4C).
12 Remarkably, no biological processes related to osteoblast differentiation, functioning or general bone
13 formation were detected in *Lrp4^{KI/KI}* osteoblasts through GO analysis, despite the HBM phenotype of
14 *Lrp4^{KI/KI}* mice that we had described previously [15].

15 Based on our RNA sequencing data and GO pathway analysis, we selected *Mmp9* (encoding matrix
16 metalloproteinase 9), *Acp5* (encoding acid phosphatase 5 or tartrate-resistant acid phosphatase (TRAP))
17 and *Tnfrsf11* (encoding the receptor activator of nuclear factor kappa-B ligand (Rankl)) for confirmation
18 with qRT-PCR in *Lrp4^{KI/KI}* osteoblasts and verification in *Sost^{-/-}* and *Sost^{-/-}; Lrp4^{KI/KI}* osteoblasts. For
19 *Mmp9*, *Acp5* and *Tnfrsf11*, we confirmed upregulation of these genes in *Lrp4^{KI/KI}* primary osteoblasts, in
20 comparison to WT osteoblasts, although this was not reaching the significance threshold for *Mmp9*
21 ($P=0.18$) and *Tnfrsf11* ($P=0.08$) (Fig. 4D). For *Acp5*, on the other hand, we detected a significant 40-fold
22 higher expression in *Lrp4^{KI/KI}* osteoblasts ($P<0.01$) than in WT osteoblasts. In *Sost^{-/-}; Lrp4^{KI/KI}*
23 osteoblasts, *Acp5* expression was still 10-fold higher than in WT osteoblasts, and significantly lower in
24 comparison to *Lrp4^{KI/KI}* osteoblasts. Although not significant due to large sample variability, it was
25 remarkable to note that *Mmp9* expression was on average 250-fold higher in *Lrp4^{KI/KI}* osteoblasts and
26 100-fold higher in *Sost^{-/-}; Lrp4^{KI/KI}* osteoblasts, compared to controls. In *Sost^{-/-}* osteoblasts, we detected
27 no differences in the expression of *Mmp9* or *Acp5*, in comparison to WT osteoblasts, whereas *Tnfrsf11*
28 expression was nearly reduced by half ($P<0.05$) (Fig. 4D). Finally, *Tnfrsf11* expression was also lower
29 in *Sost^{-/-}; Lrp4^{KI/KI}* primary osteoblasts, in comparison to both *Lrp4^{KI/KI}* ($P=0.06$) and WT osteoblasts
30 ($P<0.05$) (Fig. 4D).

31 Next, we decided to quantify the levels of TRAP (encoded by *Acp5*), RANKL and osteoprotegerin
32 (OPG) in serum of five-month-old control, *Lrp4^{KI/KI}*, *Sost^{-/-}* and *Sost^{-/-}; Lrp4^{KI/KI}* mice by using ELISA.
33 In these mice, we could not detect any differences in the individual serum levels of RANKL or OPG
34 (Fig. 5A). We then calculated the individual RANKL/OPG ratios in these mice, detecting a higher
35 RANKL/OPG ratio in *Sost^{-/-}* mice, in comparison to either *Lrp4^{KI/KI}* or *Sost^{-/-}; Lrp4^{KI/KI}* mice (Fig. 5B).
36 In contrast to our transcriptomic and qRT-PCR data, TRAP serum levels were not significantly higher

1 in *Lrp4*^{KI/KI} mice, although a higher trend could be noted, compared to controls. Interestingly,
2 significantly lower TRAP levels were detected in male and female *Sost*^{-/-} and *Sost*^{-/-}; *Lrp4*^{KI/KI} mice,
3 when compared to *Lrp4*^{KI/KI} mice (Fig. 5C), supporting our osteoclast histomorphometry data (Fig. 3C).
4 Overall, our transcriptomic and biochemical analyses of primary osteoblasts indicate that the presence
5 of the *Lrp4* p.Arg1170Gln mutation results in the upregulation of genes related to bone resorption and
6 remodeling. These markers are no longer or markedly less induced in osteoblasts or serum of *Sost*^{-/-} and
7 *Sost*^{-/-}; *Lrp4*^{KI/KI} mice, indicating a dominant countereffect by *Sost* deficiency.

1 Discussion

2 In the current study, we have generated a novel *Sost*^{-/-};*Lrp4*^{KI/KI} mouse line, and compared it to the
3 phenotype of *Sost*^{-/-} mice to evaluate synergistic effects of the inactivating p.Arg1170Trp mutation in
4 *Lrp4* on *Sost* deficiency. This compound mutant mouse model was created by crossing *Sost*^{-/-} with
5 *Lrp4*^{KI/KI} mice, of which the latter was described previously by us [15]. First of all, phenotypic
6 comparison of *Sost*^{-/-} [13] and *Lrp4*^{KI/KI} mice shows that both single mutant models present with a
7 sclerosteosis-like phenotype, although *Sost*-related HBM is more severe. Based on the mutations
8 initially found in patients with *LRP4*-related sclerosteosis, it was thought that the 3rd β-propeller domain
9 of *LRP4* was the sclerostin-interacting pocket, explaining the significant phenotypic overlap between
10 *SOST*- and *LRP4*-related sclerosteosis [6, 8, 9]. Recently, however, we have shown that compound
11 heterozygous mutations in the 1st and 3rd β-propeller domain of *LRP4* can also cause sclerosteosis [10].
12 This indicates that some residual sclerostin binding and inhibitory actions might still be present in
13 *Lrp4*^{KI/KI} mice carrying a homozygous mutation in the 3rd β-propeller, providing a possible explanation
14 why their phenotype is less severe than in *Sost*^{-/-} mice. We hypothesized that *Sost*^{-/-};*Lrp4*^{KI/KI} mice might
15 have a more severe sclerosteosis phenotype than single mutant mice. A double mutant background
16 would, in that case, further impair the inhibitory effect of sclerostin-Lrp4 on canonical WNT signaling
17 and impair the binding of other WNT inhibitors (e.g. Dickkopf1, Wise) that also bind Lrp4's
18 extracellular domain [11, 27] and might still have compensatory effects in *Sost*^{-/-} mice. Unexpectedly,
19 however, skeletal phenotyping of male *Sost*^{-/-} and *Sost*^{-/-};*Lrp4*^{KI/KI} mice showed no differences, whereas
20 female *Sost*^{-/-};*Lrp4*^{KI/KI} mice had a HBM phenotype that was less severe than that of *Sost*^{-/-} mice. This
21 effect appeared to be specific for the appendicular skeleton as differences were noticeable in the cortical
22 and trabecular bone compartment of the long bones, and not in the spine, of female *Sost*^{-/-};*Lrp4*^{KI/KI} mice.

23 The HBM phenotype of male *Sost*^{-/-};*Lrp4*^{KI/KI} mice was similar to that of male *Sost*^{-/-} mice, and more
24 severe than what we previously observed in *Lrp4*^{KI/KI} mice [15]. This finding is most likely due to a
25 dominant and robust osteoanabolic effect of sclerostin deficiency, which is reflected by higher bone
26 formation rates. We can conceptually compare these findings with a previous study, where wildtype and
27 *Lrp4* p.Arg1170Trp knock-in mice were treated with a sclerostin neutralizing monoclonal antibody (Scl-
28 mAb) [16]. Bullock and colleagues observed blunted effects of the Scl-mAb induced gain in BMD and
29 μCT-derived parameters in *Lrp4*^{KI/KI} mice, which was about half of that exhibited by wildtype mice
30 treated with Scl-mAb. They concluded that the strong anabolic effects of Scl-mAb were compromised
31 or absent in *Lrp4*^{KI/KI} mice, likely due to the mutation having similar functional (i.e., redundant) effects
32 as sclerostin neutralization. This is similar to what we have observed in male wildtype, *Sost*^{-/-} and *Sost*^{-/-};
33 *Lrp4*^{KI/KI} mice, although our findings in female mice were surprisingly different.

34 Female mice consistently exhibited a more severe skeletal phenotype than males in our study, especially
35 in the trabecular bone compartment (spine and long bones). Furthermore, long bones of female *Sost*^{-/-};
36 *Lrp4*^{KI/KI} mice were less severely and robustly affected by HBM than long bones from *Sost*^{-/-} females.

1 These findings indicate gender-specific effects on the establishment of *Sost*- and/or *Sost*;*Lrp4*-related
2 HBM phenotypes, especially in the long bones and trabecular bone compartment. Trabecular bone in
3 particular is tightly regulated by bone turnover and mechanical loading is an anabolic trigger for this
4 process, especially in the long bones [28, 29]. Our data therefore suggest that female mice are more
5 sensitive for the effects of sclerostin and *Lrp4* on this balance between osteoblasts and osteoclasts. For
6 patients with *SOST*- or *LRP4*-related forms of sclerosteosis, it is more difficult to draw conclusions
7 regarding gender-related differences, due to the low numbers of patients and phenotypic variability.

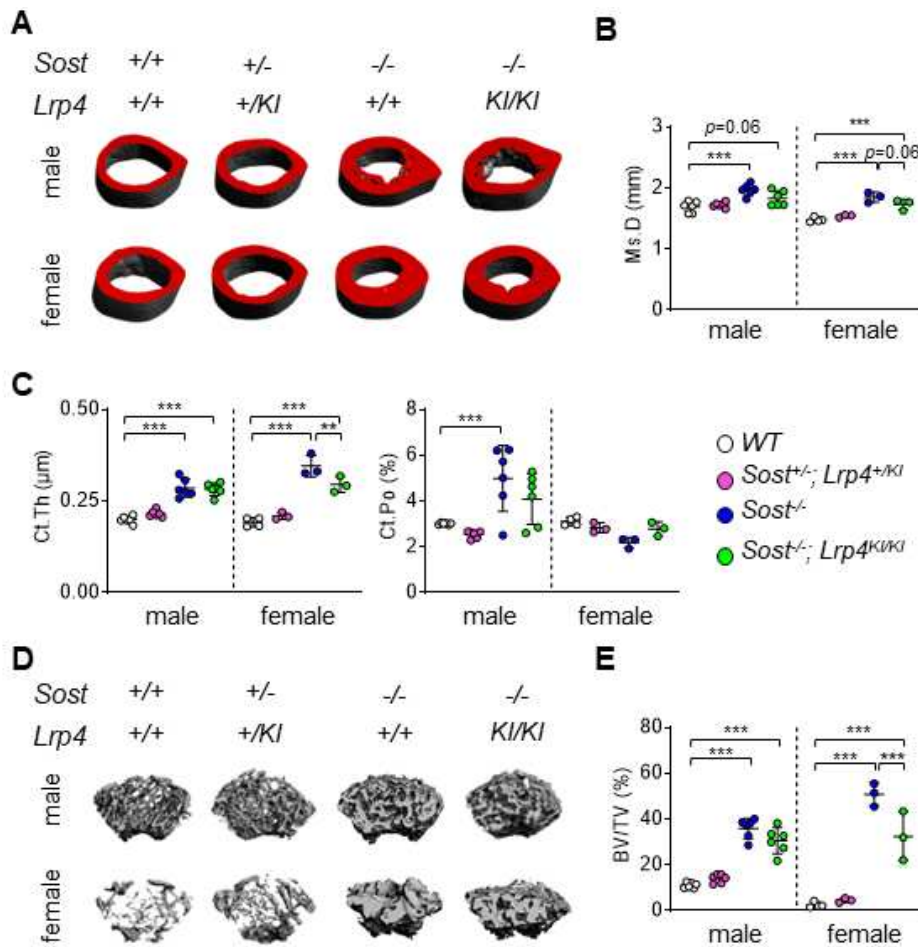
8 On a cellular level, osteoblasts have consistently been identified as the main cell type driving the
9 development of *Sost*^{-/-} or *Lrp4*^{KI/KI} phenotypes, characterized by a greater anabolic capacity of individual
10 osteoblasts (bone formation rates). As for bone resorption, osteoclast-related parameters were
11 significantly lower in *Sost*^{-/-} and *Sost*^{-/-};*Lrp4*^{KI/KI} mice, which was previously reported in *Sost*^{-/-} mice but
12 not in our *Lrp4*^{KI/KI} mice [13, 15]. In contrast, we previously noticed slightly but not significantly
13 elevated values for osteoclastic parameters in our *Lrp4*^{KI/KI} mice [15]. For the *Lrp4* knock-in mice
14 carrying the p.Arg1170Trp variant, osteoclast histomorphometry data were not included [16]. Overall,
15 it is evident that sclerostin deficiency has dominant osteoanabolic and anti-resorptive effects in male
16 and female *Sost*^{-/-} and *Sost*^{-/-};*Lrp4*^{KI/KI} mice. Also in postmenopausal women, monoclonal antibodies that
17 bind and inhibit sclerostin (e.g., Romosozumab), have also been reported to have a dual effect of
18 increasing bone formation and decreasing bone resorption [17, 30, 31]. Based on the data in this study,
19 however, the robust net gain in bone mass due to sclerostin deficiency seems partially compromised in
20 female *Sost*^{-/-};*Lrp4*^{KI/KI} mice, due to the presence of *Lrp4*^{KI/KI} alleles.

21 Contrary to our expectations, an unbiased whole-transcriptome analysis of *Lrp4*^{KI/KI} primary osteoblasts
22 revealed an upregulation of genes related to osteoclast activity and differentiation and bone remodeling.
23 While it is unclear why no genes related to osteoblastic bone formation came out of this analysis, it may
24 offer some molecular insights on the phenotypic features and differences observed in *Lrp4*^{KI/KI}, *Sost*^{-/-}
25 and *Sost*^{-/-};*Lrp4*^{KI/KI} mice. Previous studies have indicated that the function of *Lrp4* in osteoblasts is to
26 suppress bone formation and promote osteoclastogenesis and bone resorption, through inhibition of
27 canonical WNT signaling [12]. Importantly, however, these insights were obtained from experiments
28 using conditional *Lrp4* knockout mice. Based on our phenotypic, cellular and molecular data, we assume
29 that the p.Arg1170Gln variant in the 3rd β-propeller of *Lrp4* has unique effects on bone turnover, with a
30 net gain in bone mass as phenotypic outcome. Alternatively, it might also be that primary osteoblasts
31 from *Lrp4*^{KI/KI} mice do not have cell-autonomous defects on their differentiation or function, which could
32 also (partially) explain why no genes related to these processes were differentially expressed.

33 In conclusion, we did not observe an additive effect of the disease-causing p.Arg1170Trp variant in
34 *Lrp4* on *Sost* deficiency. In fact, surprisingly, the *Lrp4* variant partially mitigated the effect of the *SOST*
35 deficiency specifically in long bones of female mice. Molecular analysis of *Lrp4*^{KI/KI} osteoblasts revealed

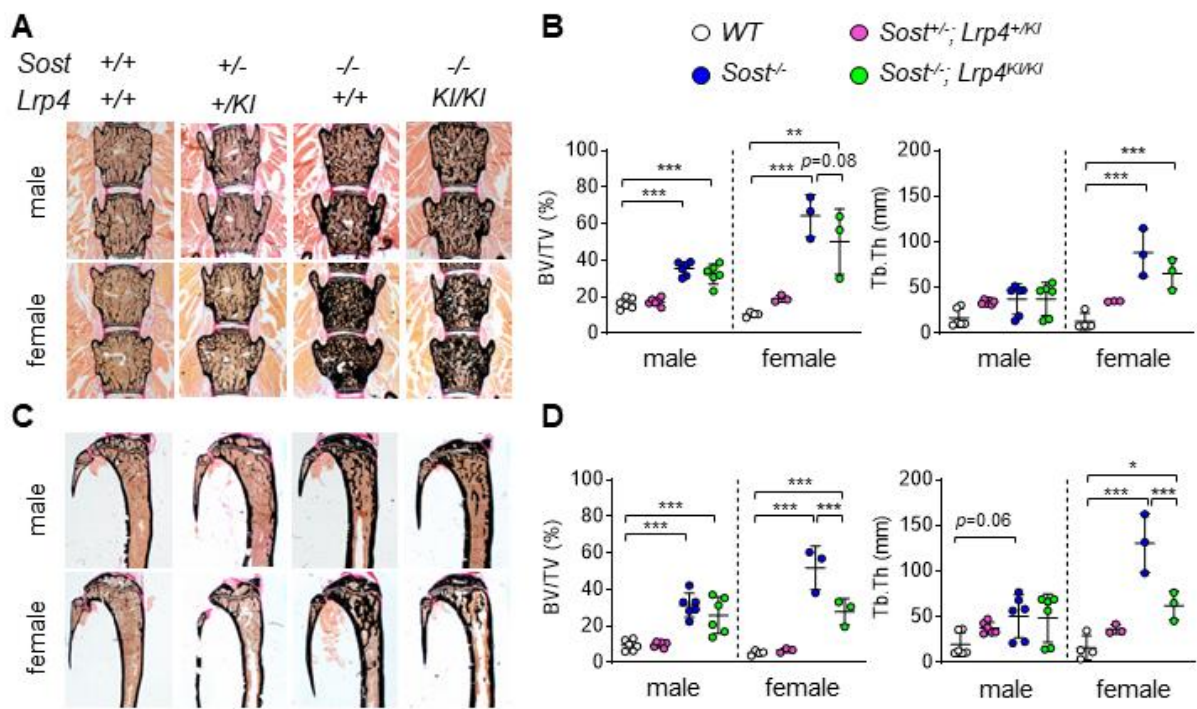
1 an unexpected increase in the expression of genes related to bone resorption and remodeling. We
2 therefore hypothesize that mouse models with two *Lrp4*^{KI} alleles rather activate bone remodeling, with
3 a net gain in bone mass, whereas sclerostin deficiency has more robust anabolic effects on bone
4 formation. Future studies, studying the molecular background of *Sost*-deficient osteoblasts/osteocytes
5 or *Lrp4*-mutant osteoblasts, with a mutation outside of the 3rd β -propeller domain, could further improve
6 our understanding of the pathogenesis of their associated high bone mass phenotypes.

1 Figures

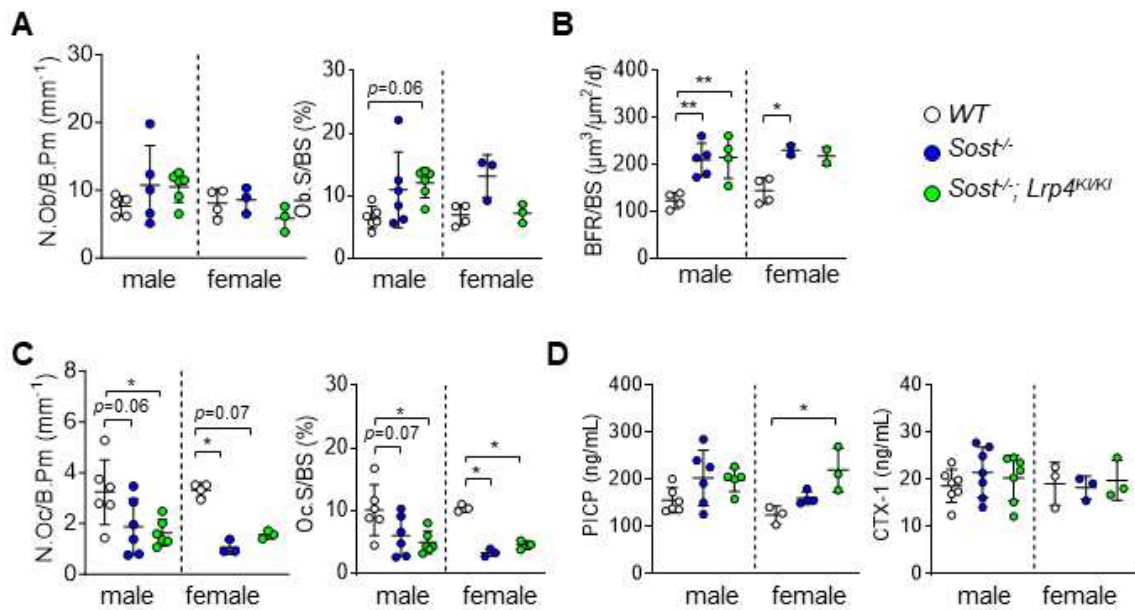


2

3 **Fig. 1** μ CT analysis of the femora demonstrates structural differences between female *Sost*^{+/-} and *Sost*^{+/-}
 4 ;*Lrp4*^{KI/KI} mice (A) Representative μ CT images of the femoral cortical bone from 5-month-old male and female
 5 control, *Sost*^{+/-}, *Sost*^{+/-};*Lrp4*^{+KI} and *Sost*^{+/-};*Lrp4*^{KI/KI} mice. (B) μ CT-based quantification of the femoral Ms.D in
 6 control (n = 6 male; n = 4 female), *Sost*^{+/-};*Lrp4*^{+KI} (n = 6 male; n = 3 female), *Sost*^{+/-} (n = 6 male; n = 3 female)
 7 and *Sost*^{+/-};*Lrp4*^{KI/KI} mice (n = 6 male; n = 3 female). (C) μ CT-based quantification of Ct.Th and Ct.Po in the
 8 femora of the same mice. (D) Representative μ CT images of the femoral trabecular bone and (E) μ CT-based
 9 quantification of the trabecular BV/TV in the same mice. Data are presented as individual data points with
 10 indication of mean \pm SD, *p*-values obtained by one-way ANOVA with Šidák's multiple comparison test. Ms.D =
 11 midshaft diameter; Ct.Th = cortical thickness; Ct.Po = cortical thickness; BV/TV = bone volume per tissue volume.



1
2 **Fig. 2 Histomorphometry confirms structural differences between female *Sost*^{-/-} and *Sost*^{-/-};*Lrp4*^{KI/KI} mice in**
3 **the tibia, but not in spine (A)** Representative images after Von Kossa/van Gieson staining of lumbar spine
4 sections of 5-month-old control, *Sost*^{-/-}, *Sost*^{+/-};*Lrp4*^{+/-KI} and *Sost*^{-/-};*Lrp4*^{KI/KI} mice. **(B)** Quantification of the
5 trabecular BV/TV and thickness in lumbar spine sections of control (n = 6 male; n = 4 female), *Sost*^{+/-};*Lrp4*^{+/-KI} (n
6 = 6 male; n = 3 female), *Sost*^{-/-} (n = 6 male; n = 3 female) and *Sost*^{-/-};*Lrp4*^{KI/KI} mice (n = 6 male; n = 3 female). **(C)**
7 Representative images of tibial sections after Von Kossa/van Gieson staining from 5-month old male and female
8 control, *Sost*^{-/-} and *Sost*^{-/-};*Lrp4*^{KI/KI} mice. **(D)** Quantification of the trabecular BV/TV and thickness in tibial sections
9 of the same mice. Data are presented as individual data points with indication of mean ± SD, *p*-values obtained by
10 one-way ANOVA with Šidák's multiple comparison test. BV/TV = bone volume per tissue volume; Tb.Th =
11 trabecular thickness.



1

2 **Fig. 3 Cellular and dynamic histomorphometry demonstrates higher bone formation rates and lower bone**

3 **resorption parameters in *Sost*^{-/-} and *Sost*^{-/-}; *Lrp4*^{KI/KI} mice** (A) Histomorphometric quantification of N.Ob/B.Pm

4 and Ob.S/BS in lumbar spine sections of 5-month-old control (n = 5 male; n = 4 female), *Sost*^{-/-} (n = 6 male; n = 3

5 female) and *Sost*^{-/-}; *Lrp4*^{KI/KI} mice (n = 6 male; n = 3 female). (B) Dynamic histomorphometry of the BFR/BS on

6 lumbar spine sections of the same mice. (C) Histomorphometric quantification of the osteoclast number and

7 covered surface in lumbar spine sections of the same mice. (D) Biochemical analysis of serum parameters for bone

8 formation (PICP) and bone resorption (CTX-1) the same mice. Data are presented as individual data points with

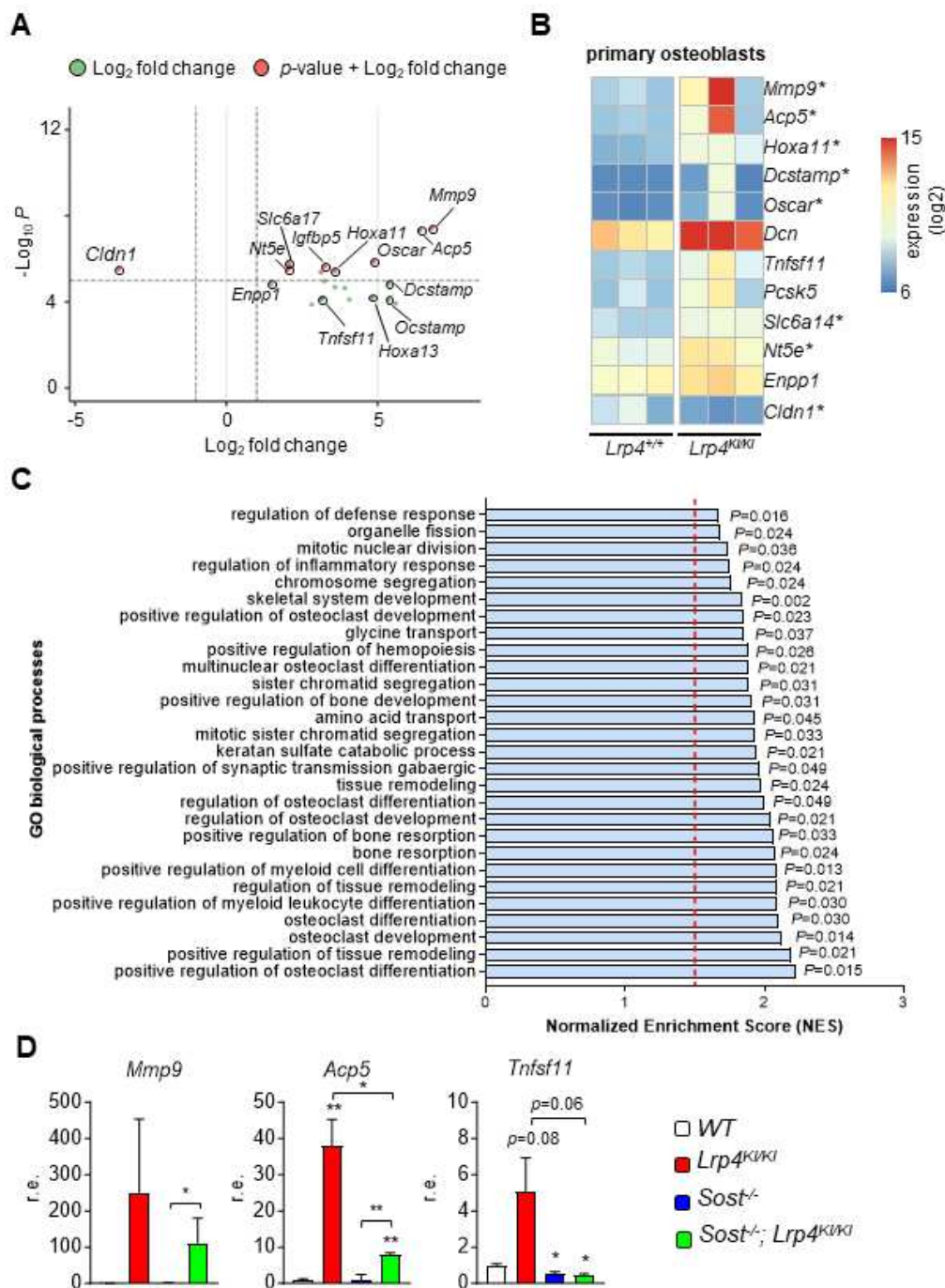
9 indication of mean \pm SD, *p*-values obtained by one-way ANOVA with Šidák's multiple comparison test. BV/TV

10 = bone volume per tissue volume; Tb.Th = trabecular thickness. N.Ob/B.Pm = number of osteoblasts per bone

11 perimeter; Ob.S/BS = osteoblast surface per bone surface; BFR/BS = bone formation rate per bone surface;

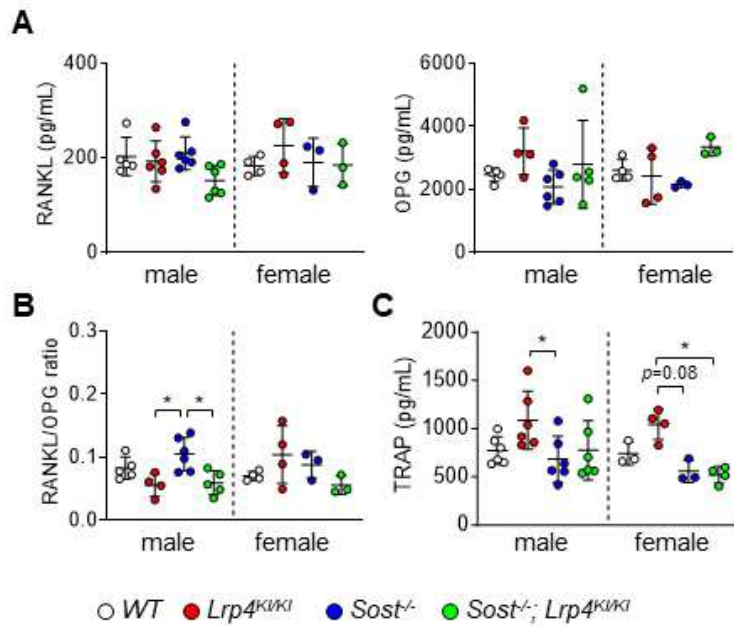
12 N.Oc/B.Pm = number of osteoclasts per bone perimeter; Oc.S/BS = osteoclast surface per bone surface; PICP =

13 procollagen type-I C-terminal peptide; CTX-1 = collagen type 1 cross-linked C-telopeptide.



1
2 **Fig. 4 Transcriptome analysis of $Lrp4^{KI/KI}$ primary osteoblasts demonstrates upregulation of genes involved**
3 **in bone resorption and bone remodeling (A)** Volcano plot of all the differentially expressed genes in three
4 independent sets of $Lrp4^{+/+}$ versus $Lrp4^{KI/KI}$ primary osteoblasts. **(B)** Heat map showing the expression of a
5 selection of differentially expressed genes in $Lrp4^{KI/KI}$ primary osteoblasts, in comparison to $Lrp4^{+/+}$ primary
6 osteoblasts. An asterisk indicates a significant differential expression. **(C)** Gene Ontology (GO) enrichment
7 analysis of genes differentially expressed in $Lrp4^{KI/KI}$ primary osteoblasts, compared to $Lrp4^{+/+}$ primary
8 osteoblasts. The values behind the bar graph are adjusted p -values based on the hypergeometric test. The vertical
9 red dotted line indicates the threshold value for the normalized enrichment score (NES > +1.5). **(D)** qRT-PCR
10 analysis of *Mmp9*, *Acp5* and *Tnfsf11* in primary osteoblasts from wildtype, $Lrp4^{KI/KI}$, $Sost^{-/-}$ and $Sost^{-/-}; Lrp4^{KI/KI}$

1 mice. Data are presented as bar graphs with mean \pm SD, p -values obtained by one-way ANOVA with Šidák's
 2 multiple comparison test.



3
 4 **Fig. 5 Biochemical verification of RANKL, OPG and TRAP in serum of single and double mutant mouse**
 5 **models (A)** ELISA-based quantification of RANKL and OPG levels in the serum of 5-month-old control (n = 5
 6 male; n = 4 female), *Lrp4^{KI/KI}* (n = 4 - 6 male; n = 4 female), *Sost^{-/-}* (n = 4-6 male; n = 4 female) and *Sost^{-/-}; Lrp4^{KI/KI}*
 7 mice (n = 6 male; n = 3 female). **(B)** Calculated RANKL/OPG ratios from these mice based on their individual
 8 RANKL and OPG serum levels. **(C)** ELISA-based quantification of TRAP levels in the serum of these mice. Data
 9 are presented as individual data points with indication of mean \pm SD, p -values obtained by one-way ANOVA with
 10 Šidák's multiple comparison test.

1 Figure Legends

2 **Fig. 1 μ CT analysis of the femora demonstrates structural differences between female $Sost^{-/-}$ and $Sost^{-/-};Lrp4^{KI/KI}$ mice** (A) Representative μ CT images of the femoral cortical bone from 5-month-old male and female
3 control, $Sost^{-/-}$, $Sost^{+/-};Lrp4^{+/-KI}$ and $Sost^{-/-};Lrp4^{KI/KI}$ mice. (B) μ CT-based quantification of the femoral Ms.D in
4 control (n = 6 male; n = 4 female), $Sost^{+/-};Lrp4^{+/-KI}$ (n = 6 male; n = 3 female), $Sost^{-/-}$ (n = 6 male; n = 3 female)
5 and $Sost^{-/-};Lrp4^{KI/KI}$ mice (n = 6 male; n = 3 female). (C) μ CT-based quantification of Ct.Th and Ct.Po in the
6 femora of the same mice. (D) Representative μ CT images of the femoral trabecular bone and (E) μ CT-based
7 quantification of the trabecular BV/TV in the same mice. Data are presented as individual data points with
8 indication of mean \pm SD, p -values obtained by one-way ANOVA with Šidák's multiple comparison test. Ms.D =
9 midshaft diameter; Ct.Th = cortical thickness; Ct.Po = cortical thickness; BV/TV = bone volume per tissue volume.
10

11
12 **Fig. 2 Histomorphometry confirms structural differences between female $Sost^{-/-}$ and $Sost^{-/-};Lrp4^{KI/KI}$ mice in**
13 **the tibia, but not in spine** (A) Representative images after Von Kossa/van Gieson staining of lumbar spine
14 sections of 5-month-old control, $Sost^{-/-}$, $Sost^{+/-};Lrp4^{+/-KI}$ and $Sost^{-/-};Lrp4^{KI/KI}$ mice. (B) Quantification of the
15 trabecular BV/TV and thickness in lumbar spine sections of control (n = 6 male; n = 4 female), $Sost^{+/-};Lrp4^{+/-KI}$ (n
16 = 6 male; n = 3 female), $Sost^{-/-}$ (n = 6 male; n = 3 female) and $Sost^{-/-};Lrp4^{KI/KI}$ mice (n = 6 male; n = 3 female). (C)
17 Representative images of tibial sections after Von Kossa/van Gieson staining from 5-month old male and female
18 control, $Sost^{-/-}$ and $Sost^{-/-};Lrp4^{KI/KI}$ mice. (D) Quantification of the trabecular BV/TV and thickness in tibial sections
19 of the same mice. Data are presented as individual data points with indication of mean \pm SD, p -values obtained by
20 one-way ANOVA with Šidák's multiple comparison test. BV/TV = bone volume per tissue volume; Tb.Th =
21 trabecular thickness.

22 **Fig. 3 Cellular and dynamic histomorphometry demonstrates higher bone formation rates and lower bone**
23 **resorption parameters in $Sost^{-/-}$ and $Sost^{-/-};Lrp4^{KI/KI}$ mice** (A) Histomorphometric quantification of N.Ob/B.Pm
24 and Ob.S/BS in lumbar spine sections of 5-month-old control (n = 5 male; n = 4 female), $Sost^{-/-}$ (n = 6 male; n = 3
25 female) and $Sost^{-/-};Lrp4^{KI/KI}$ mice (n = 6 male; n = 3 female). (B) Dynamic histomorphometry of the BFR/BS on
26 lumbar spine sections of the same mice. (C) Histomorphometric quantification of the osteoclast number and
27 covered surface in lumbar spine sections of the same mice. (D) Biochemical analysis of serum parameters for bone
28 formation (PICP) and bone resorption (CTX-1) the same mice. Data are presented as individual data points with
29 indication of mean \pm SD, p -values obtained by one-way ANOVA with Šidák's multiple comparison test. BV/TV
30 = bone volume per tissue volume; Tb.Th = trabecular thickness. N.Ob/B.Pm = number of osteoblasts per bone
31 perimeter; Ob.S/BS = osteoblast surface per bone surface; BFR/BS = bone formation rate per bone surface;
32 N.Oc/B.Pm = number of osteoclasts per bone perimeter; Oc.S/BS = osteoclast surface per bone surface; PICP =
33 procollagen type-I C-terminal peptide; CTX-1 = collagen type 1 cross-linked C-telopeptide.
34

35 **Fig. 4 Transcriptome analysis of $Lrp4^{KI/KI}$ primary osteoblasts demonstrates upregulation of genes involved**
36 **in bone resorption and bone remodeling** (A) Volcano plot of all the differentially expressed genes in three
37 independent sets of $Lrp4^{+/-}$ versus $Lrp4^{KI/KI}$ primary osteoblasts. (B) Heat map showing the expression of a
38 selection of differentially expressed genes in $Lrp4^{KI/KI}$ primary osteoblasts, in comparison to $Lrp4^{+/-}$ primary

1 osteoblasts. An asterisk indicates a significant differential expression. (C) Gene Ontology (GO) enrichment
2 analysis of genes differentially expressed in *Lrp4^{KI/KI}* primary osteoblasts, compared to *Lrp4^{+/+}* primary
3 osteoblasts. The values behind the bar graph are adjusted *p*-values based on the hypergeometric test. The vertical
4 red dotted line indicates the threshold value for the normalized enrichment score (NES > +1.5). (D) qRT-PCR
5 analysis of *Mmp9*, *Acp5* and *Tnfsf11* in primary osteoblasts from wildtype, *Lrp4^{KI/KI}*, *Sost^{-/-}* and *Sost^{-/-};Lrp4^{KI/KI}*
6 mice. Data are presented as bar graphs with mean ± SD, *p*-values obtained by one-way ANOVA with Šidák's
7 multiple comparison test.

8

9 **Fig. 5 Biochemical verification of RANKL, OPG and TRAP in serum of single and double mutant mouse**
10 **models (A)** ELISA-based quantification of RANKL and OPG levels in the serum of 5-month-old control (n = 5
11 male; n = 4 female), *Lrp4^{KI/KI}* (n = 4 - 6 male; n = 4 female), *Sost^{-/-}* (n = 4-6 male; n = 4 female) and *Sost^{-/-};Lrp4^{KI/KI}*
12 mice (n = 6 male; n = 3 female). (B) Calculated RANKL/OPG ratios from these mice based on their individual
13 RANKL and OPG serum levels. (C) ELISA-based quantification of TRAP levels in the serum of these mice. Data
14 are presented as individual data points with indication of mean ± SD, *p*-values obtained by one-way ANOVA with
15 Šidák's multiple comparison test.

1 **References**

- 2 1. Huybrechts Y, Mortier G, Boudin E, Van Hul W (2020) WNT Signaling and Bone: Lessons
3 From Skeletal Dysplasias and Disorders. *Front Endocrinol (Lausanne)* 11:165
- 4 2. Bergen DJM, Maurizi A, Formosa MM, McDonald GLK, El-Gazzar A, Hassan N, Brandi ML,
5 Riancho JA, Rivadeneira F, Ntzani E, Duncan EL, Gregson CL, Kiel DP, Zillikens MC,
6 Sangiorgi L, Hogler W, Duran I, Makitie O, Van Hul W, Hendrickx G (2023) High Bone Mass
7 Disorders: New Insights From Connecting the Clinic and the Bench. *J Bone Miner Res* 38:229-
8 247
- 9 3. Hamersma H, Gardner J, Beighton P (2003) The natural history of sclerosteosis. *Clin Genet*
10 63:192-197
- 11 4. Balemans W, Ebeling M, Patel N, Van Hul E, Olson P, Dioszegi M, Lacza C, Wuyts W, Van
12 Den Ende J, Willems P, Paes-Alves AF, Hill S, Bueno M, Ramos FJ, Tacconi P, Dikkers FG,
13 Stratakis C, Lindpaintner K, Vickery B, Foerzler D, Van Hul W (2001) Increased bone density
14 in sclerosteosis is due to the deficiency of a novel secreted protein (SOST). *Hum Mol Genet*
15 10:537-543
- 16 5. Brunkow ME, Gardner JC, Van Ness J, Paeper BW, Kovacevich BR, Proll S, Skonier JE, Zhao
17 L, Sabo PJ, Fu Y, Alisch RS, Gillett L, Colbert T, Tacconi P, Galas D, Hamersma H, Beighton
18 P, Mulligan J (2001) Bone dysplasia sclerosteosis results from loss of the SOST gene product,
19 a novel cystine knot-containing protein. *Am J Hum Genet* 68:577-589
- 20 6. Leupin O, Piters E, Halleux C, Hu S, Kramer I, Morvan F, Bouwmeester T, Schirle M, Bueno-
21 Lozano M, Fuentes FJ, Itin PH, Boudin E, de Freitas F, Jennes K, Brannetti B, Charara N,
22 Ebersbach H, Geisse S, Lu CX, Bauer A, Van Hul W, Kneissel M (2011) Bone overgrowth-
23 associated mutations in the LRP4 gene impair sclerostin facilitator function. *J Biol Chem*
24 286:19489-19500
- 25 7. van Lierop AH, Hamdy NA, Hamersma H, van Bezooijen RL, Power J, Loveridge N,
26 Papapoulos SE (2011) Patients with sclerosteosis and disease carriers: human models of the
27 effect of sclerostin on bone turnover. *J Bone Miner Res* 26:2804-2811
- 28 8. Ohkawara B, Cabrera-Serrano M, Nakata T, Milone M, Asai N, Ito K, Ito M, Masuda A, Ito Y,
29 Engel AG, Ohno K (2014) LRP4 third beta-propeller domain mutations cause novel congenital
30 myasthenia by compromising agrin-mediated MuSK signaling in a position-specific manner.
31 *Hum Mol Genet* 23:1856-1868
- 32 9. Fijalkowski I, Geets E, Steenackers E, Van Hoof V, Ramos FJ, Mortier G, Fortuna AM, Van
33 Hul W, Boudin E (2016) A Novel Domain-Specific Mutation in a Sclerosteosis Patient Suggests
34 a Role of LRP4 as an Anchor for Sclerostin in Human Bone. *J Bone Miner Res* 31:874-881
- 35 10. Huybrechts Y, Boudin E, Hendrickx G, Steenackers E, Hamdy N, Mortier G, Martinez Diaz-
36 Guerra G, Bracamonte MS, Appelman-Dijkstra NM, Van Hul W (2022) Identification of
37 Compound Heterozygous Variants in LRP4 Demonstrates That a Pathogenic Variant outside
38 the Third beta-Propeller Domain Can Cause Sclerosteosis. *Genes (Basel)* 13:80
- 39 11. Choi HY, Dieckmann M, Herz J, Niemeier A (2009) Lrp4, a novel receptor for Dickkopf 1 and
40 sclerostin, is expressed by osteoblasts and regulates bone growth and turnover in vivo. *PLoS*
41 *One* 4:e7930
- 42 12. Xiong L, Jung JU, Wu H, Xia WF, Pan JX, Shen C, Mei L, Xiong WC (2015) Lrp4 in osteoblasts
43 suppresses bone formation and promotes osteoclastogenesis and bone resorption. *Proc Natl*
44 *Acad Sci U S A* 112:3487-3492
- 45 13. Kramer I, Loots GG, Studer A, Keller H, Kneissel M (2010) Parathyroid hormone (PTH)-
46 induced bone gain is blunted in SOST overexpressing and deficient mice. *J Bone Miner Res*
47 25:178-189

- 1 14. Li X, Ominsky MS, Niu QT, Sun N, Daugherty B, D'Agostin D, Kurahara C, Gao Y, Cao J,
2 Gong J, Asuncion F, Barrero M, Warmington K, Dwyer D, Stolina M, Morony S, Sarosi I,
3 Kostenuik PJ, Lacey DL, Simonet WS, Ke HZ, Paszty C (2008) Targeted deletion of the
4 sclerostin gene in mice results in increased bone formation and bone strength. *J Bone Miner Res*
5 23:860-869
- 6 15. Boudin E, Yorgan T, Fijalkowski I, Sonntag S, Steenackers E, Hendrickx G, Peeters S, De Mare
7 A, Vervaeke B, Verhulst A, Mortier G, D'Haese P, Schinke T, Van Hul W (2017) The
8 Lrp4R1170Q Homozygous Knock-In Mouse Recapitulates the Bone Phenotype of Sclerosteosis
9 in Humans. *J Bone Miner Res* 32:1739-1749
- 10 16. Bullock WA, Hoggatt AM, Horan DJ, Elmendorf AJ, Sato AY, Bellido T, Loots GG, Pavalko
11 FM, Robling AG (2019) Lrp4 Mediates Bone Homeostasis and Mechanotransduction through
12 Interaction with Sclerostin In Vivo. *iScience* 20:205-215
- 13 17. Cosman F, Crittenden DB, Adachi JD, Binkley N, Czerwinski E, Ferrari S, Hofbauer LC, Lau
14 E, Lewiecki EM, Miyachi A, Zerbin CA, Milmont CE, Chen L, Maddox J, Meisner PD,
15 Libanati C, Grauer A (2016) Romosozumab Treatment in Postmenopausal Women with
16 Osteoporosis. *N Engl J Med* 375:1532-1543
- 17 18. Hendrickx G, Boudin E, Van Hul W (2015) A look behind the scenes: the risk and pathogenesis
18 of primary osteoporosis. *Nat Rev Rheumatol* 11:462-474
- 19 19. Chang MK, Kramer I, Huber T, Kinzel B, Guth-Gundel S, Leupin O, Kneissel M (2014)
20 Disruption of Lrp4 function by genetic deletion or pharmacological blockade increases bone
21 mass and serum sclerostin levels. *Proc Natl Acad Sci U S A* 111:E5187-5195
- 22 20. Percie du Sert N, Ahluwalia A, Alam S, Avey MT, Baker M, Browne WJ, Clark A, Cuthill IC,
23 Dirnagl U, Emerson M, Garner P, Holgate ST, Howells DW, Hurst V, Karp NA, Lazic SE,
24 Lidster K, MacCallum CJ, Macleod M, Pearl EJ, Petersen OH, Rawle F, Reynolds P, Rooney
25 K, Sena ES, Silberberg SD, Steckler T, Wurbel H (2020) Reporting animal research:
26 Explanation and elaboration for the ARRIVE guidelines 2.0. *PLoS Biol* 18:e3000411
- 27 21. Yorgan TA, Peters S, Jeschke A, Benisch P, Jakob F, Amling M, Schinke T (2015) The Anti-
28 Osteoanabolic Function of Sclerostin Is Blunted in Mice Carrying a High Bone Mass Mutation
29 of Lrp5. *J Bone Miner Res* 30:1175-1183
- 30 22. Bouxsein ML, Boyd SK, Christiansen BA, Guldberg RE, Jepsen KJ, Muller R (2010)
31 Guidelines for assessment of bone microstructure in rodents using micro-computed
32 tomography. *J Bone Miner Res* 25:1468-1486
- 33 23. Albers J, Keller J, Baranowsky A, Beil FT, Catala-Lehnen P, Schulze J, Amling M, Schinke T
34 (2013) Canonical Wnt signaling inhibits osteoclastogenesis independent of osteoprotegerin. *J*
35 *Cell Biol* 200:537-549
- 36 24. Parfitt AM, Drezner MK, Glorieux FH, Kanis JA, Malluche H, Meunier PJ, Ott SM, Recker RR
37 (1987) Bone histomorphometry: standardization of nomenclature, symbols, and units. Report
38 of the ASBMR Histomorphometry Nomenclature Committee. *J Bone Miner Res* 2:595-610
- 39 25. Hendrickx G, Borra VM, Steenackers E, Yorgan TA, Hermans C, Boudin E, Waterval JJ, Jansen
40 IDC, Aydemir TB, Kamerling N, Behets GJ, Plumeyer C, D'Haese PC, Busse B, Everts V,
41 Lammens M, Mortier G, Cousins RJ, Schinke T, Stokroos RJ, Manni JJ, Van Hul W (2018)
42 Conditional mouse models support the role of SLC39A14 (ZIP14) in Hyperostosis Cranialis
43 Interna and in bone homeostasis. *PLoS Genet* 14:e1007321
- 44 26. Love MI, Huber W, Anders S (2014) Moderated estimation of fold change and dispersion for
45 RNA-seq data with DESeq2. *Genome Biol* 15:550
- 46 27. Ohazama A, Johnson EB, Ota MS, Choi HY, Porntaveetus T, Oommen S, Itoh N, Eto K, Gritli-
47 Linde A, Herz J, Sharpe PT (2008) Lrp4 modulates extracellular integration of cell signaling
48 pathways in development. *PLoS One* 3:e4092

- 1 28. Ozcivici E, Luu YK, Adler B, Qin YX, Rubin J, Judex S, Rubin CT (2010) Mechanical signals
2 as anabolic agents in bone. *Nat Rev Rheumatol* 6:50-59
- 3 29. Papachroni KK, Karatzas DN, Papavassiliou KA, Basdra EK, Papavassiliou AG (2009)
4 Mechanotransduction in osteoblast regulation and bone disease. *Trends Mol Med* 15:208-216
- 5 30. McClung MR, Grauer A, Boonen S, Bolognese MA, Brown JP, Diez-Perez A, Langdahl BL,
6 Reginster JY, Zanchetta JR, Wasserman SM, Katz L, Maddox J, Yang YC, Libanati C, Bone
7 HG (2014) Romosozumab in postmenopausal women with low bone mineral density. *N Engl J*
8 *Med* 370:412-420
- 9 31. Padhi D, Jang G, Stouch B, Fang L, Posvar E (2011) Single-dose, placebo-controlled,
10 randomized study of AMG 785, a sclerostin monoclonal antibody. *J Bone Miner Res* 26:19-26